

Spin-polarized electronic surface states of Re(0001): an ab-initio investigation

Andrea Urru¹ and Andrea Dal Corso^{1,2}

¹*International School for Advanced Studies (SISSA),
Via Bonomea 265, 34136 Trieste (Italy).*

²*IOM-CNR Trieste (Italy).*

We study the electronic structure of the Re(0001) surface by means of ab-initio techniques based on the Fully Relativistic (FR) Density Functional Theory (DFT) and the Projector Augmented-Wave (PAW) method. We identify the main surface states and resonances and study in detail their energy dispersion along the main symmetry lines of the SBZ. Moreover, we discuss the effect of spin-orbit coupling on the energy splittings and the spin-polarization of the main surface states and resonances. Whenever possible, we compare the results with previously studied heavy metals surfaces. We find empty resonances, located below a gap similar to the L-gap of the (111) fcc surfaces, that have a downward dispersion and cross the Fermi level, similarly to the recently studied Os(0001) surface. Their spin polarization at the Fermi level is similar to that predicted by the Rashba model, but the usual level crossing at $\bar{\Gamma}$ is not found with our slab thickness. Moreover, for selected states, we follow the spin polarization along the high symmetry lines, discussing its behavior with respect to \mathbf{k}_{\parallel} , the wave-vector parallel to the surface.

I. INTRODUCTION

The presence of electronic states localized in the last few atomic layers of a solid, namely surface states, can give surfaces properties different from the bulk.¹ Moreover, since surfaces lack inversion symmetry, even non-magnetic (i.e. time-reversal invariant) materials can have surface states with a non-vanishing spin polarization. Hence, surface states might be practically useful for instance in spintronics applications, and it is worthwhile to characterize them.

The energy dispersion of surface states with respect to \mathbf{k}_{\parallel} , the wave-vector parallel to the surface, and in some cases also their spin polarization, have been analyzed for many surfaces of different materials, by both theoretical and experimental techniques (Density Functional Theory, DFT,²⁻⁹ and photoelectron spectroscopy, PES,¹⁰⁻¹⁹ angular- and spin-resolved). For instance, for the heavy metal surfaces, the L-gap surface states are well known.^{2-9,11,12,15,18} They show a characteristic split parabolic energy dispersion, that can be interpreted by the Rashba model²⁰ as a relativistic effect due to spin-orbit coupling.

Recently, we found theoretically that Os(0001) surface⁹ should host Rashba split surface states around $\bar{\Gamma}$, below a gap similar to the L-gap of the (111) fcc surfaces, but with an inverted dispersion as in Ir(111).⁸ Moreover, energy splittings due to spin-orbit coupling are present in other surface states of Os(0001), such as the S_2 , S'_3 , and S_4 states analyzed in Ref. 9.

Re(0001) is another interesting surface used²¹⁻²³ both as a support for other metallic layers and as a reactive catalytic surface. Very recently, it has been shown that artificially constructed Fe chains on top of Re(0001) surface exhibit a spin spiral state.²⁴ Though Re(0001) has been widely studied, surprisingly little information is available about its electronic structure. Being similar to the other surfaces discussed above, Re(0001) could have

states similar to the Rashba split surface states with an inverted dispersion as, e.g., in Ir(111) and Os(0001). Also the other surface states could be similar, but both the energy dispersion and their spin polarization, are poorly known.

In this work, we study by ab-initio techniques the electronic structure of Re(0001). We characterize its main surface states and follow, for the most interesting ones, the average direction of the spin polarization as a function of \mathbf{k}_{\parallel} . About $\bar{\Gamma}$, we find Rashba-like states with negative curvature, which cross the Fermi energy, and we characterize their spin texture at the Fermi level. We find also several states already familiar from the study of the other surfaces. We analyze the main surface states that appear in the electronic band structure: in particular, at variance with Au(111), Pt(111), and Ir(111), but as in Os(0001), we do not find the S_8 Dirac-like surface states, studied in Ref. 7.

The paper is organized as follows: in Section II, we describe the methods and the computational parameters. In Section III, we present the Re(0001) electronic band structure and analyze the main surface states and resonances. In Section IV, we discuss the spin polarization of some selected states and finally, in Section V, we present our conclusions.

II. METHOD

First-principle calculations were performed by means of DFT^{25,26} within the Local Density Approximation (LDA) scheme, as implemented in the Quantum ESPRESSO^{27,28} and **thermo_pw**.²⁹ packages The Perdew and Zunger's³⁰ parameterization for the exchange and correlation energy is used. Spin-orbit coupling effects are included by using the Fully Relativistic (FR) PAW method,³¹ with 5d and 6s valence electrons and 5s and 5p semicore states (Pseudopotential Re.rel-pz-spnpaw_psl.1.0.0.UPF from pslibrary.1.0.0^{32,33}). Calculations

lations on the bulk system, were performed with an hexagonal close-packed (hcp) structure at the theoretical LDA lattice constants: $a = 5.175$ a.u., $c = 8.338$ a.u. ($c/a = 1.611$), which are respectively 0.8% and 1% smaller than experiment ($a_{exp} = 5.217$ a.u., $c_{exp} = 8.425$ a.u.).³⁴ The surface has been simulated by both a 24-layers and a 25-layers slab perpendicular to the [0001] direction in order to check the stability of the results with respect to the breaking of the inversion symmetry. The slab replicas have been separated by a vacuum space of 44 a.u.. The slab crystal structure has been obtained from the bulk, with a further relaxation along the [0001] direction, which has the most relevant effects on the first three atomic layers: in particular, the distance between the first two layers decreases by 5.4% with respect to the idealized interlayer distance in the bulk, while the distance between the second and the third layer increases by 2.9%. At a first stage, we performed a calculation with a starting non-zero magnetization, but the self-consistent ground state of the slab ended up to be non magnetic. The pseudo wavefunctions are expanded in a plane waves basis set with a kinetic energy cut-off of 60 Ry, while the charge density with a cut-off of 400 Ry. BZ integrations were performed using a shifted uniform Monkhorst-Pack³⁵ \mathbf{k} -point mesh of $16 \times 16 \times 1$ points for the slab and $16 \times 16 \times 10$ points for the bulk. The presence of a Fermi surface has been dealt with by the Methfessel-Paxton method³⁶ with a smearing parameter $\sigma = 0.02$ Ry. With these parameters the total energy is converged within 10^{-3} Ry and the crystal parameters within 10^{-3} Å. In Figs. 1a-b we show the first two atomic layers of the 24-layers slab and the 25-layers slab, respectively. The 24-layers slab has a D_{3d} point group. In particular, the z axis, normal to the surface, is a $\bar{3}$ rotoinversion axis, while the axes [100], [110], and [010] in Fig. 1a are two-fold rotation axes. There are also three mirror planes, $(\bar{1}20)$, $(2\bar{1}0)$, and (110) shown in Fig. 1a. The 25-layers slab has instead, a D_{3h} point group. The z axis is a $\bar{6}$ axis, while the axes [210], [120], and $[\bar{1}10]$, shown in Fig. 1b, are two-fold rotation axes. Moreover, there are three mirror planes, whose traces coincide with the C_2 axes [210], [120], and $[\bar{1}10]$. The electronic band structure was calculated along the path $\bar{\Gamma} - \bar{K} - \bar{M} - \bar{\Gamma}$ (that is along the \bar{T} , \bar{T}' , and $\bar{\Sigma}$ high-symmetry lines) of the Surface Brillouin Zone (SBZ), shown in Figs. 1c-d. The small point group of \mathbf{k} of the two slabs is indicated in the band structure in Figs. 2a and 2b, both for the high symmetry points ($\bar{\Gamma}$, \bar{K} , and \bar{M}) and for the high symmetry lines (\bar{T} , \bar{T}' , and $\bar{\Sigma}$). In particular, for the 24-layers slab, at $\bar{\Gamma}$, \bar{K} , and \bar{M} the small group of \mathbf{k} is D_{3d} , D_3 , and C_{2h} , respectively. Along the high symmetry lines \bar{T} , \bar{T}' , and $\bar{\Sigma}$ it is C_2 , C_2 , and C_s , respectively. Along \bar{T} the rotation axis coincides with the x -axis, while along \bar{T}' the rotation axis is the $[\bar{1}20]$ axis, shown in Fig. 1c. Finally, along $\bar{\Sigma}$ the trace of the mirror plane of C_s is $\bar{\Sigma}$. On the other hand, for the 25-layers slab, at $\bar{\Gamma}$, \bar{K} , and \bar{M} the small group of \mathbf{k} is D_{3h} , C_{3h} , and C_{2v} , respectively, while along the high symmetry lines \bar{T} , \bar{T}' ,

and $\bar{\Sigma}$ it is C_s , C_s , and C_{2v} , respectively. In particular, along \bar{T} and \bar{T}' the mirror plane is σ_h . The two slabs have more symmetry elements than the Re(0001) surface, since they have symmetry operations that exchange the two surfaces. Removing these elements, the surface point group is C_{3v} , while the small groups of \mathbf{k} are C_{3v} , C_3 , and C_s for $\bar{\Gamma}$, \bar{K} , and \bar{M} respectively and C_1 , C_1 , and C_s along \bar{T} , \bar{T}' , and $\bar{\Sigma}$. Actually, they are the same for both slabs.

III. RESULTS

In this section, we analyze the Re(0001) 24-layers slab FR band structure, shown in Fig. 2a. We characterize the main surface states, indicated with red dots in Fig. 2a, and compare them with Os(0001) and other previously studied surfaces (e.g. Au(111), Pt(111), and Ir(111)). We use the same names as in Ref. 9. Moreover, at the end of the section we discuss the band structure of a 25-layers slab (Fig. 2 b).

We start our analysis from the $\bar{\Gamma}$ point, where we find two gaps in the PBS. Taking the Fermi energy as a reference, the first is located 4 eV above it and the second approximately from -7 eV to -3 eV. The first gap, higher in energy, is similar to the L-gap of the fcc surfaces and is found in Os(0001) as well. It extends partly along the \bar{T} and $\bar{\Sigma}$ lines. The second gap, deeper in energy, extends up to half of the \bar{T} line and along the whole $\bar{\Sigma}$ line. Similarly to Os(0001) and Ir(111), but at variance with Au(111) and Pt(111), no surface states are found in the L-gap. Below the L-gap, near the Fermi energy, we found two couples of states (L in Fig. 2a) that transform as the Γ_4^- and Γ_4^+ representations of the D_{3d} group. Their energy dispersion around $\bar{\Gamma}$ is parabolic with negative curvature, as for the Rashba split states in Os(0001) and Ir(111). In these surfaces we could fit their dispersion with the equation:

$$E_{\pm} = \frac{\hbar^2}{2m^*} k_{\parallel}^2 \pm \gamma_{SO} k_{\parallel}, \quad (1)$$

where k_{\parallel} is the modulus of the wave-vector parallel to the surface, m^* is the effective electron mass and γ_{SO} is the spin-orbit coupling parameter. However, here their dispersions do not cross at $\bar{\Gamma}$, as shown in Fig. 3 a, and even neglecting this splitting it is not possible to fit them with Eq. (1). Nevertheless, at the Fermi energy the two states show a splitting along k_{\parallel} , due to spin-orbit coupling: indeed, a comparison with the Scalar Relativistic (SR) band structure (Fig. 3 b), shows that this splitting emerges only in the FR picture. Moreover, the spin texture of the L states at the Fermi energy is well predicted by the Rashba model (see Section IV for more details), so they behave as Rashba states. In Fig. 4a we show the contour plots and the planar average of the sum of the charge densities at $\bar{\Gamma}$ for the L_a states, the couple higher in energy. The contour plots suggest that it has mainly s

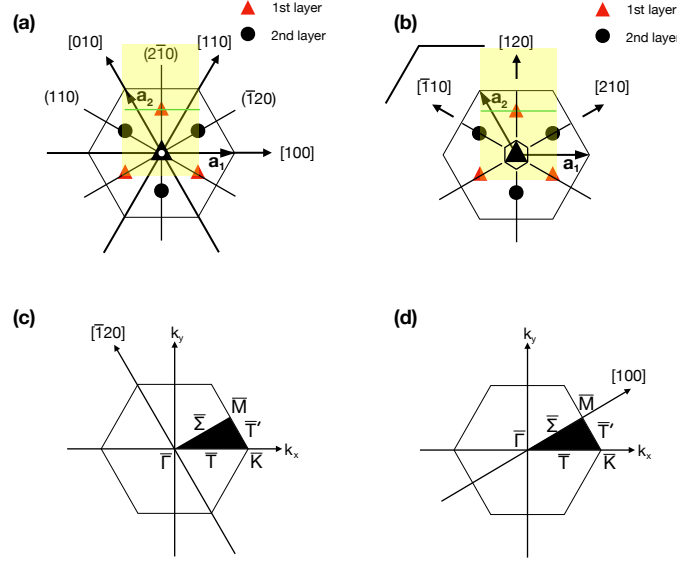


Figure 1. (a)-(b) Positions of the atoms in the first two atomic layers of the Re(0001) 24-layers and 25-layers slab, respectively. Arrows and solid lines indicate the C_2 rotation axes and the mirror planes, respectively. (c)-(d) Surface Brillouin Zone of Re(0001) 24-layers and 25-layers slab, respectively. The Irreducible Brillouin Zone (IBZ) and the path used to plot the electronic band structure are shown. The $[\bar{1}20]$ and $[100]$ axes are the two-fold rotation axes of the small groups of \mathbf{k}_{\parallel} along \bar{T}' for the 24-layers and along $\bar{\Sigma}$ for the 25-layers slab, respectively.

Surface State	\mathbf{k}_{\parallel}	ε (eV) Re(0001)	ε (eV) Os(0001)	ε (eV) Ir(111)	ε (eV) Pt(111)	ε (eV) Au(111)	Small group of \mathbf{k}_{\parallel}			Symmetry	
L	$\bar{\Gamma}$	0.68	0.08	-0.31	0.1	-0.5	D_{3d}	$[D_{3h}]$	(C_{3v})	Γ_4^-, Γ_4^+	$[\Gamma_7, \Gamma_8]$ (Γ_4)
S_2	$\bar{\Gamma}$	-6.77	-7.87	-8.0	-7.4	-7.6				Γ_4^+, Γ_4^-	$[\Gamma_7, \Gamma_8]$ (Γ_4)
S_{13}	$\bar{\Gamma}$	3.35	1.55	—	—	—				Γ_4^+, Γ_4^-	$[\Gamma_7, \Gamma_8]$ (Γ_4)
S'_{3a}	\bar{K}	2.58	1.07	—	—	—	D_3	$[C_{3h}]$	(C_3)	$\Gamma_5 \oplus \Gamma_6$	$[\Gamma_{11} \oplus \Gamma_{12}]$ ($2\Gamma_6$)
S'_{3b}	\bar{K}	2.49	0.97	—	—	—				Γ_4	$[\Gamma_7 \oplus \Gamma_9]$ ($\Gamma_4 \oplus \Gamma_5$)
S'_{3c}	\bar{K}	2.42	—	—	—	—				Γ_4	$[\Gamma_7 \oplus \Gamma_9]$ ($\Gamma_4 \oplus \Gamma_5$)
S_{4a}	\bar{K}	-1.30	-2.35	-2.7	-2.8	-3.7				Γ_4	$[\Gamma_8 \oplus \Gamma_{10}]$ ($\Gamma_4 \oplus \Gamma_5$)
S_{4b}	\bar{K}	-1.72	-2.74	-3.1	-3.1	-4.0				Γ_4	$[\Gamma_7 \oplus \Gamma_9]$ ($\Gamma_4 \oplus \Gamma_5$)
S_{4c}	\bar{K}	-1.73	-2.72	-3.1	-3.1	-4.0				$\Gamma_5 \oplus \Gamma_6$	$[\Gamma_{11} \oplus \Gamma_{12}]$ ($2\Gamma_6$)
S_{4d}	\bar{K}	-1.82	-2.99	-3.5	-3.7	-4.7				Γ_4	$[\Gamma_8 \oplus \Gamma_{10}]$ ($\Gamma_4 \oplus \Gamma_5$)
S_{12}	\bar{M}	1.68	0.86	—	—	—	C_{2h}	$[C_{2v}]$	(C_s)	$\Gamma_3^+ \oplus \Gamma_4^+$	$[\Gamma_5]$ ($\Gamma_3 \oplus \Gamma_4$)
S_7	\bar{M}	-5.80	-7.00	-6.7	-6.3	-6.6				$\Gamma_3^+ \oplus \Gamma_4^+, \Gamma_3^- \oplus \Gamma_4^-$	$[\Gamma_5]$ ($\Gamma_3 \oplus \Gamma_4$)
S_{10}	$0.6 \bar{K}$	1.42	-0.24	-0.8	-1.2	—	C_2	$[C_s]$	(C_1)	$\Gamma_3 \oplus \Gamma_4$	$[\Gamma_3 \oplus \Gamma_4]$ (Γ_2)

Table I. Energy and symmetry properties of the surface states discussed in the paper, for the Re(0001), Os(0001), Ir(111), Pt(111), and Au(111) surfaces. The reported symmetry refers to the 24-layers slab. In square brackets, the symmetry for the 25-layers slab, in parentheses, the symmetry relevant for the surface.

character hybridized with some d states. The planar average is maximum around the surface and shows a very slow decay towards the center of the slab, indicating that the L states are resonances. The gap at $\bar{\Gamma}$ could have several causes: among them, the evident hybridization with bulk states, possibly together with the finite size of the slab. Yet, a calculation with a 40-layers slab shows that the gap at $\bar{\Gamma}$ between L_a and L_b is the same as for the 24-layers slab, thus finite-size effects do not play a relevant role in this case.

At lower energies at $\bar{\Gamma}$, there are two couples of states in a PBS gap, similar to the previously studied S_2 states of the other metal surfaces. At $\bar{\Gamma}$, they have symmetry Γ_4^+ and Γ_4^- . Their energy dispersion has a positive curvature and can be fitted with (1), with: $\gamma_{SO} = (0.200 \pm 0.005) \times 10^{-9}$ eV cm and $m^*/m = (0.661 \pm 0.003)$, with identical values, within the error bar, along \bar{T} and $\bar{\Sigma}$. In particular, γ_{SO} is 30 % lower than in Os(0001), while the effective mass is approximately 10 % lower. The charge density contours and planar average of the

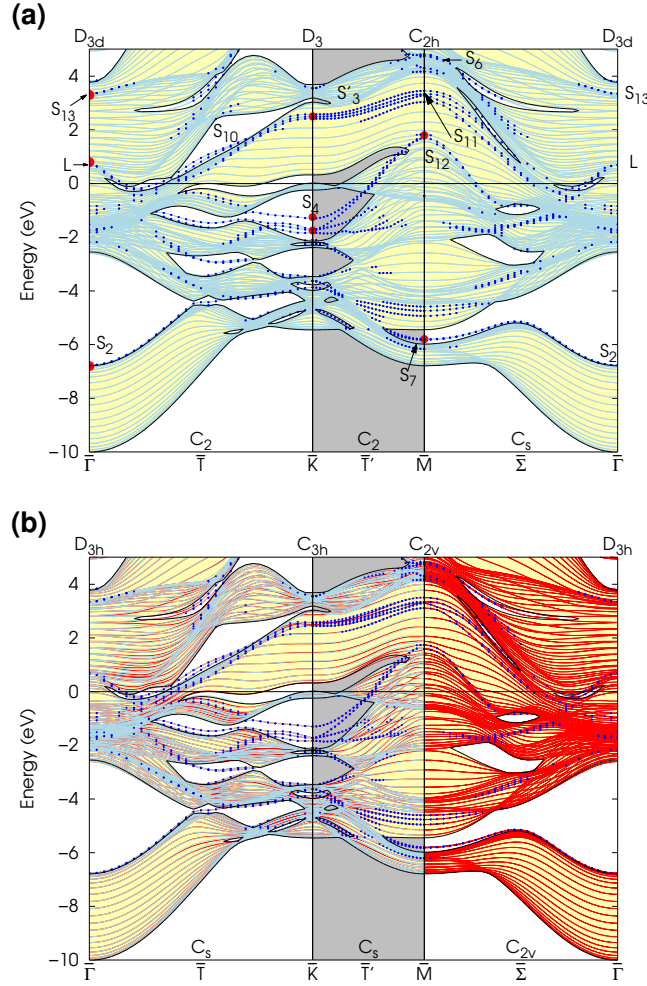


Figure 2. (Color online) LDA FR-PAW surface band structure of Re(0001). (a) 24-layers slab band structure, (b) 25-layers slab band structure. The yellow region is the Projected Band Structure (PBS), the light blue and red lines are the slab electronic states and the blue dots indicate surface states or resonances, defined as those having a charge density greater than 0.35 on the last two atomic layers of both surfaces. Energies are measured with respect to the Fermi energy, and the energy maximum in the figure is the computed work function (5.01 eV). Red dots in (a) indicate the states shown in Figs. 4 and 5.

S_{2a} states, those higher in energy, are shown in Fig. 4b. The states are surface states mainly localized on the first two atomic layers.

Finally, at $\bar{\Gamma}$ there are two couples of empty localized surface states called S_{13} , which have been characterized in Os(0001) surface. At $\bar{\Gamma}$ they transform as the Γ_4^+ and Γ_4^- representations of the D_{3d} group. Similarly to Os(0001), they are resonances and they have mainly d character, with main contributions from the first two atomic layers (Fig. 4c).

The states L , S_2 , and S_{13} extend partially also along the \bar{T} line, where they all transform as the $\Gamma_3 \oplus \Gamma_4$ representation of the C_2 group. Along \bar{T} we find some PBS gaps as well: the widest ones host the S_{10} , S_4 , and the previously mentioned S_2 states. The S_{10} states are two couples of degenerate states with symmetry $\Gamma_3 \oplus \Gamma_4$. They cross the Fermi level around $k_{\parallel} = 0.51 \text{ \AA}^{-1}$. As

in Pt(111), Ir(111), and Os(0001), they merge with the S'_3 states at \bar{K} . The S_4 states are located inside a PBS gap, they cross the \bar{K} point and extend along the \bar{T}' line as well. They have symmetry $\Gamma_3 \oplus \Gamma_4$.

At \bar{K} we find four main gaps in the PBS: the highest in energy is located above 3.5 eV, the second one crosses the Fermi level and does not host any surface state, the third one contains the S_4 states, while the fourth one extends down to -3.5 eV. The main surface states at \bar{K} are the S'_3 and S_4 states. S'_3 are made up of three couples of empty states, that are named S'_{3a} , S'_{3b} , and S'_{3c} in decreasing order of energy. S'_{3a} transforms as the $\Gamma_5 \oplus \Gamma_6$ representation of the D_3 group, while S'_{3b} and S'_{3c} have symmetry Γ_4 . As in Os(0001), they are not in a PBS gap, they are localized in the first two atomic layers and project mainly on $d_{3z^2-r^2}$ states, as can be seen from the charge density contour lines shown in Fig. 4d.

The S_4 states are located in the PBS gap found at

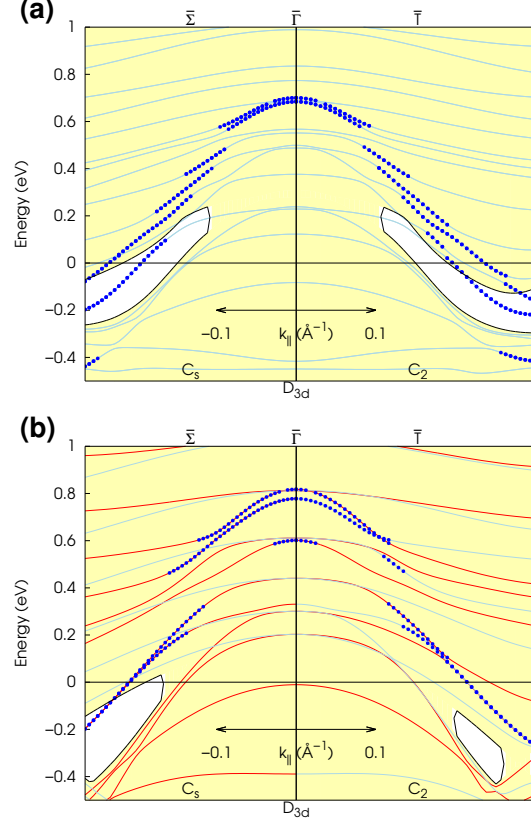


Figure 3. Magnification of the electronic band structure around $\bar{\Gamma}$ in the FR (a) and SR (b) case. The L states are shown with blue dots.

$-2 \text{ eV} < E < -0.3 \text{ eV}$. S_{4a} , S_{4b} , and S_{4d} transform as the representation Γ_4 , while S_{4c} transforms as $\Gamma_5 \oplus \Gamma_6$. In Fig. 5 we show their charge density, which is peaked on the top atomic layer, with a small contribution on the third atomic layer for S_{4a} , S_{4b} , and S_{4d} . They have very similar features in Os(0001), though S_{4b} and S_{4c} exchange their character, as can be argued from the symmetry and the charge density plots.

The PBS gaps and surface states described at \bar{K} extend also along the \bar{T}' line. Both S'_3 and S_4 states, along \bar{T}' have symmetry $\Gamma_3 \oplus \Gamma_4$ of the C_2 group. Moreover, S_{4b} and S_{4c} anticross near \bar{K} ($k \approx 1.53 \text{ \AA}^{-1}$), similarly to Os(0001). Along \bar{T}' , near \bar{M} , we find another PBS gap, located around -6 eV , that hosts the S_7 states. It extends up to \bar{M} and along the whole $\bar{\Sigma}$ line, as well as the S_7 states, that connect to the S_2 states at \bar{M} .

At \bar{M} , besides the previously mentioned PBS gap and S_7 states, we find the S_{12} states. They are a couple of degenerate states with symmetry $\Gamma_3^+ \oplus \Gamma_4^+$ and project on many d states (Fig. 4 e). The S_7 states, instead, are made up of two couples of states, that belong to the representations $\Gamma_3^+ \oplus \Gamma_4^+$ and $\Gamma_3^- \oplus \Gamma_4^-$ of the group C_{2h} , respectively. They have a strong contribution to the charge density (Fig. 4f) coming from $d_{x^2-y^2}$ and d_{xy} orbitals lo-

calized in the first atomic layer.

The band structure of the 25-layers slab (Fig. 2 b) is overall very similar to the one of the 24-layers slab and the surface states are located at the same energies in both slabs. Nevertheless there are minor differences, due to the different symmetries of the two slabs. In particular, since the 25-layers slab lacks inversion symmetry (its point group is D_{3h}), only the $k - -k$ Kramers degeneracy remains, and a spin splitting may appear, along some lines. This is the case of the lines \bar{T} and \bar{T}' , in which states of different symmetry (in our case, even and odd with respect to the mirror plane σ_h) are split. The spin splitting is different for different states: it can be very small as, e.g., $\approx 10^{-6} \text{ eV}$ for the S_4 states, or larger as $\approx 0.03 \text{ eV}$ for the S'_3 states, and it decreases increasing the slab thickness.³⁷ At variance with the states along \bar{T} and \bar{T}' , the states along $\bar{\Sigma}$ are doubly degenerate because the C_{2v} double group has only one two-dimensional irreducible representation, Γ_5 .

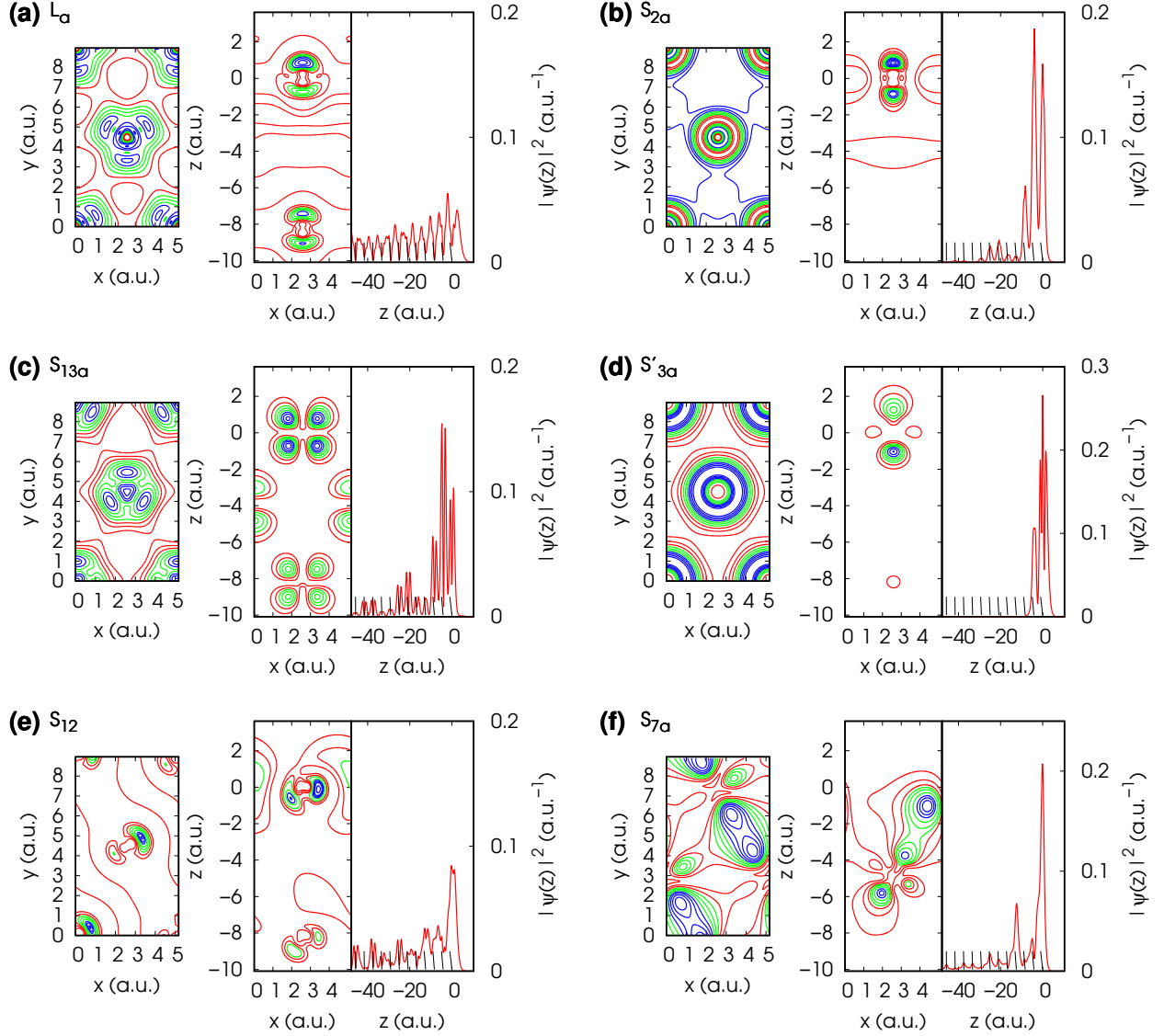


Figure 4. Contour plots and planar average of the charge density corresponding to the selected FR surface states indicated with red dots in Fig. 2. The left subplot shows the charge density contour plot in the yellow region in Fig. 1a, on the top atomic layer of the slab. The central subplot shows the contour plot in a plane perpendicular to the slab, whose trace is the green line in Fig. 1a. The contours are equally spaced and are indicated with different colors (red, green, and blue in increasing order of charge density). The first three atomic layers are shown. The right subplot shows the planar average of the charge density in one half of the slab. The vacuum is on the right; the z ticks represent the positions of the atomic layers.

IV. SPIN POLARIZATION: RESULTS AND DISCUSSION

In this section we discuss the spin polarization of some of the surface states found above. The spin polarization can be obtained integrating the planar average of the magnetization density over half slab:

$$m_\alpha = \int_0^{L/2} m_\alpha(z) dz, \quad (2)$$

where the zero of z is taken at the center of the slab and L is its length along z , including vacuum. $m_\alpha(z)$ in Eq. 2 is the planar average of the magnetization density $m_{\mathbf{k}n}^\alpha(\mathbf{r})$ associated to the Bloch state $\langle \mathbf{r} | \Psi_{\mathbf{k}n\sigma} \rangle$ and is defined as:

$$m_\alpha(z) = \int_A m_{\mathbf{k}n}^\alpha(x, y, z) dx dy, \quad (3)$$

where A is the yellow shaded region shown in Fig. 1a, and

$$m_{\mathbf{k}n}^\alpha(\mathbf{r}) = \mu_B \sum_n \sum_{\sigma_1, \sigma_2} \langle \Psi_{\mathbf{k}n\sigma_1} | \mathbf{r} \rangle \sigma_\alpha^{\sigma_1 \sigma_2} \langle \mathbf{r} | \Psi_{\mathbf{k}n\sigma_2} \rangle, \quad (4)$$

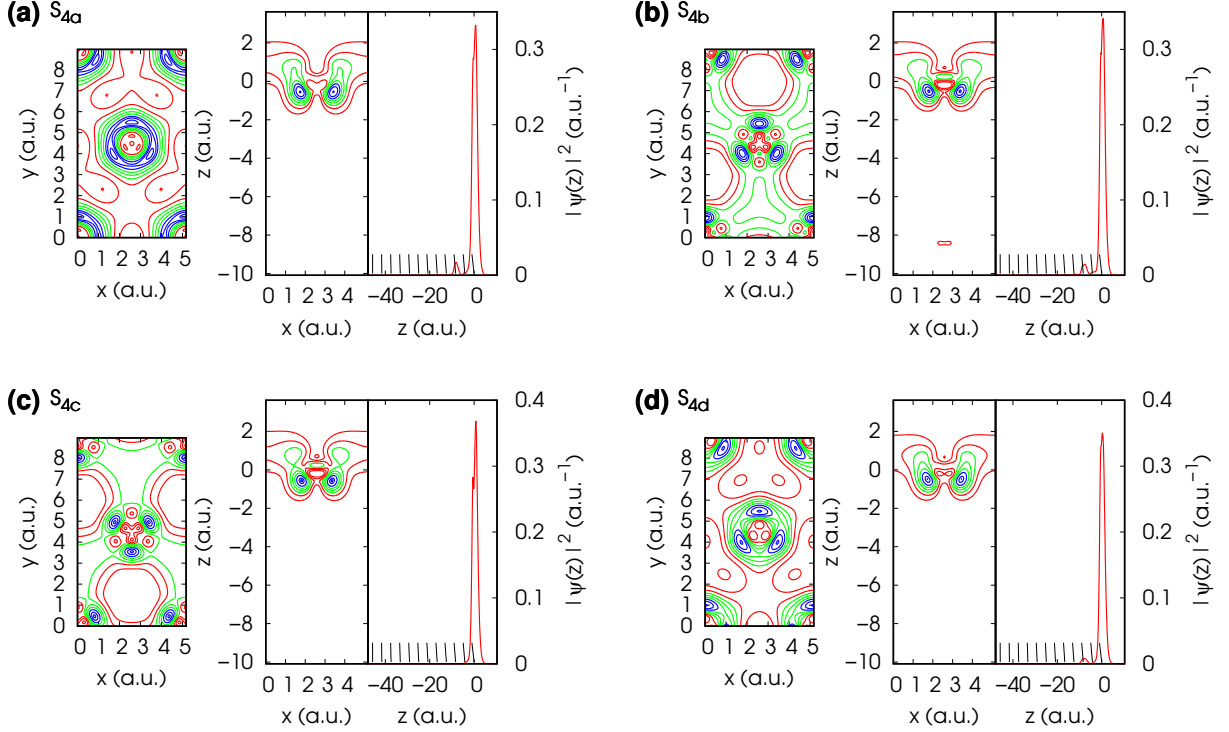


Figure 5. Contour plots and planar average of the charge density of the S_4 surface states at \bar{K} . The organization of the subplots is the same as in Fig. 4.

where μ_B is the Bohr magneton and σ_α are the Pauli matrices. The sum over σ_1 and σ_2 is over the spin, while the sum over n is over degenerate states (see Ref. 9 for more details).

We start our discussion from the L states. In particular, we consider their contribution to the Fermi surface and their spin texture at the Fermi energy. The results are shown in Fig. 6. The Fermi surface of the slab is shown in Fig. 6a, while the contour levels of the L states, shown in Fig. 6b (compared with the SBZ) are magnified in Fig. 6c: they have been obtained with a cubic interpolation of the energies of the states computed in a 14×14 square mesh of \mathbf{k} points centered in $\bar{\Gamma}$. The spin polarization, computed via Eq. (2), is represented by arrows whose length is proportional to the component of the spin parallel to the surface. The arrows are colored according to the magnitude of the spin polarization (Eq. 2) perpendicular to the surface, as indicated by the color map in the Figure. The L_b states have a circular Fermi surface, whereas the shape of the L_a states is more influenced by the underlying lattice. The component of the spin polarization parallel to the surface is perpendicular to the wavevector for both states, and it rotates clockwise and counter-clockwise for the two states, respectively. This is in agreement with the prediction of the Rashba model,²⁰ so the L states appear as Rashba split states at the Fermi level, although it has not been possible to fit their energy dispersion with Eq. (1). In particular, given the dependence of the Rashba spin texture

on the sign of both the effective mass and the spin-orbit coupling parameter,³⁸ our results are consistent with a Rashba model with $\gamma_{SO} > 0$. Due to the presence of the underlying atomic layers, the spin polarization shows a non vanishing component perpendicular to the surface. As shown in Fig. 6d, this component oscillates around zero along the contour levels, with a period of $2\pi/3$ as a consequence of the symmetry of the lattice, with opposite phase for L_a and L_b . Similar effects can be simulated also in the Rashba model by introducing hexagonal warping effects.^{39,40}

Along the \bar{T} and \bar{T}' high symmetry lines the spin polarization can rotate in a plane perpendicular to the line, as explained in Refs. 9, 41. In this work we consider the rotation of the spin polarization of the states S'_3 , S_{10} (Fig. 7), and S_4 (Fig. 8).

The S'_3 states (Figs. 7a-c) have been studied along the whole \bar{T}' line: at \bar{K} the states have only a non-zero z (perpendicular to the surface) component of the spin polarization, due to symmetry constraints, while at \bar{M} their spin polarization vanishes because \bar{M} is a time-reversal invariant point. The spin polarization of S'_{3a} is mainly perpendicular to the surface: the z component decreases along the \bar{T}' line, in a similar fashion as in Os(0001). The S'_{3b} states show a more pronounced rotation: the z component changes sign along the high symmetry line, and the component perpendicular to \bar{T}' spans a wide range of values, at variance with Os(0001). Finally, the S'_{3c} states have a rotating spin along \bar{T}' , which always points

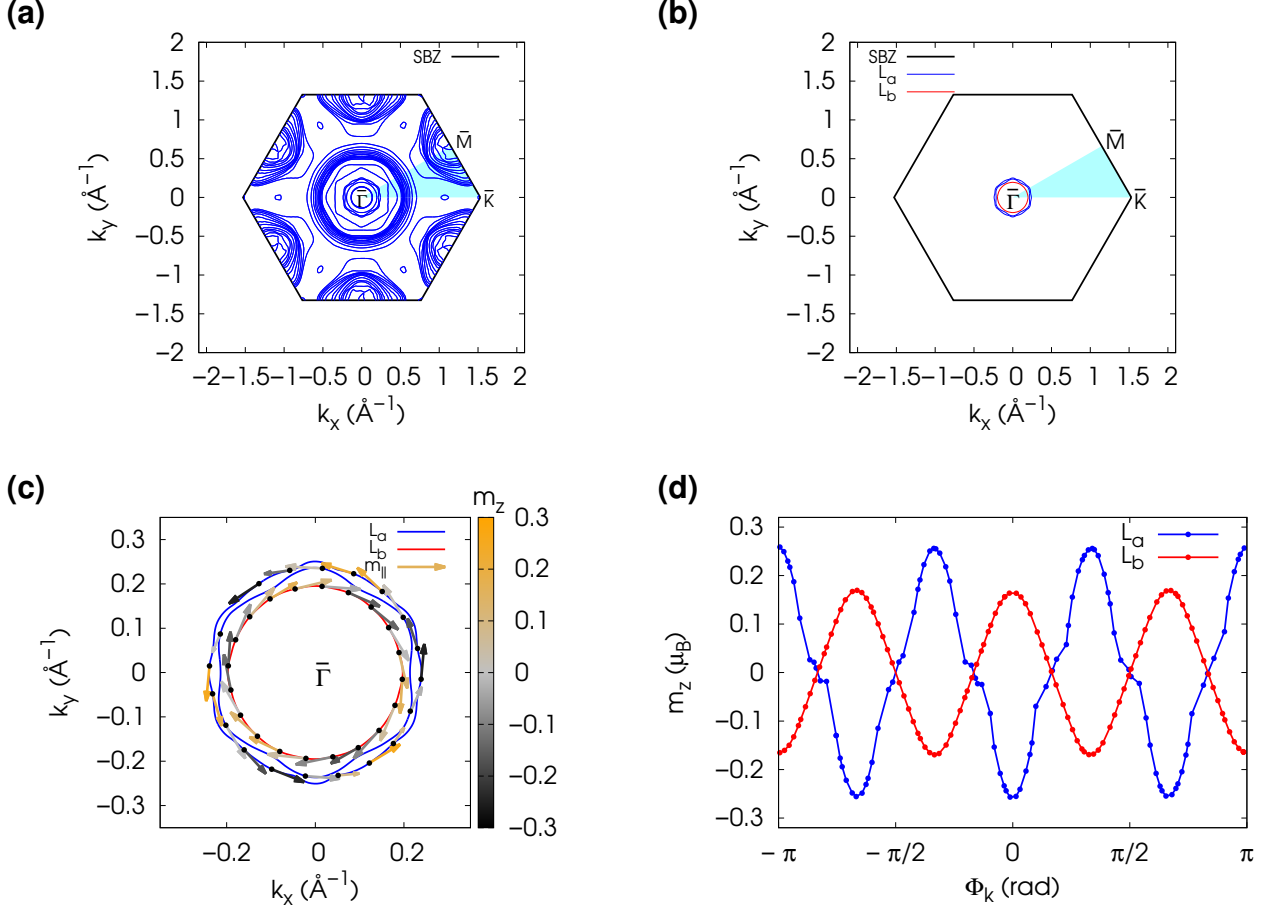


Figure 6. (a) Fermi surface of the Re(0001) 24-layers slab. The light blue region is the Irreducible Brillouin Zone (IBZ). (b) The $L_{a,b}$ surface states contours shown in comparison with the SBZ. (c) Magnification of the $L_{a,b}$ surface states contours at the Fermi energy. The black dots indicate the surface states, the arrows indicate the spin polarization parallel to the surface, and they are colored depending on the magnitude of the z component of the spin polarization. (d) z component of the spin polarization for the states $L_{a,b}$ as a function of $\Phi_k = \tan^{-1}(k_y/k_x)$.

towards the center of the slab: its behaviour is similar to what shown in Os(0001).

The S_{10} states show a smooth evolution of the spin polarization in the region $0.55 \text{ \AA}^{-1} < k_{\parallel} < 1 \text{ \AA}^{-1}$, as shown in Figs. 7d,e: in particular, S_{10a} and S_{10b} have opposite spin. Around $k_{\parallel} \approx 0.55 \text{ \AA}^{-1}$ and $k_{\parallel} \approx 1 \text{ \AA}^{-1}$ the spin polarization rotates more rapidly, because the two states anti-cross. Overall, their behaviour is similar to that shown by Os(0001).

Finally, the S_4 states (Fig. 8) show a spin texture along \bar{T} and \bar{T}' very similar to Os(0001). In particular, the smoothest behaviour is shown by S_{4d} , for which the spin always points towards the slab. S_{4b} and S_{4c} have a rapidly varying spin, even in a very narrow range of k_{\parallel} as shown in Fig. 8 b-c, due to their mixing and anticrossing around \bar{K} : a comparison with Os(0001) shows that their features are exchanged, as pointed out by their symmetry (see Table I).

Similar calculations have been performed for the 25-layers slab as well. The results are very similar to those discussed above, in particular for the S_4 and S_{10} states, which have the same energy dispersion in the two systems. Instead, the spin polarization of the S'_3 states shows a somehow different behavior, characterized by more rapid variations, which might be due to the mixing of the states caused by their non-negligible spin splitting. However, as pointed out by remark 37, the spin splitting decreases, though slowly, with increasing slab thickness, so we expect a better agreement using a thicker slab.

V. CONCLUSIONS

We discussed the electronic structure of Re(0001) surface. We analyzed its main surface states and resonances, focusing on the contours and planar average of their

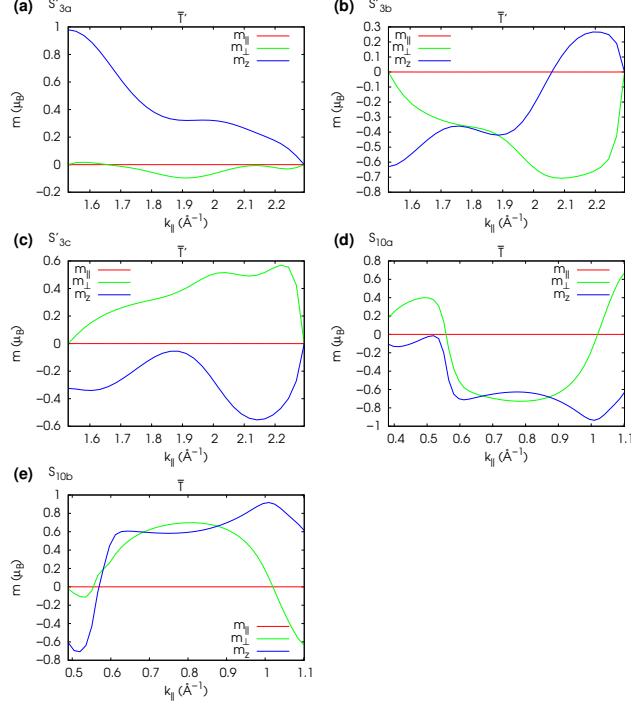


Figure 7. Spin polarization components as a function of \mathbf{k}_{\parallel} for the FR surface states $S'_{3a,b,c}$ and $S'_{10a,b}$. m_{\parallel} and m_{\perp} are the spin polarization components parallel to the surface: they are parallel and perpendicular to the high symmetry line, respectively. m_z is the component perpendicular to the surface.

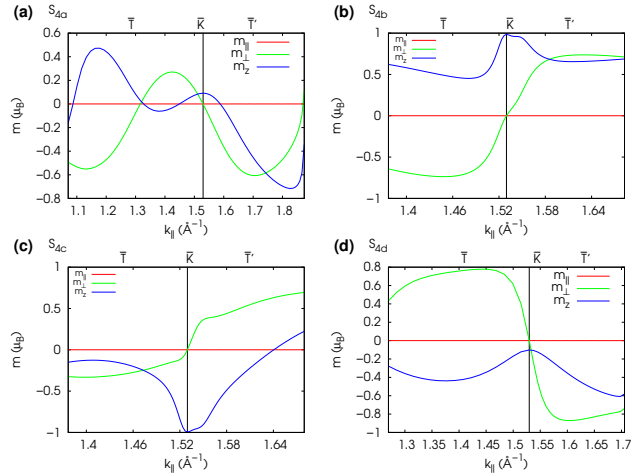


Figure 8. Spin polarization components as a function of \mathbf{k}_{\parallel} for the FR surface states $S_{4a,b,c,d}$. The convention on m_{\parallel} , m_{\perp} , and m_z is the same as in Fig. 7

charge density. At $\bar{\Gamma}$ we found a gap similar to the L-gap of the (111) fcc surfaces. Like in the recently studied Os(0001) and at variance with other well known metal surfaces (e.g. Au(111)), this gap does not contain any surface state. Two states that cross the Fermi level, with

the same nature as the L-gap surface state of Au(111), have been found: their spin texture at the Fermi energy is similar to the one predicted by the Rashba model, though the energy dispersion crossing predicted at $\bar{\Gamma}$ has not been found. Rashba split states are actually of interest because

they can have relevant applications in spintronics^{42,43} and recently their engineering has been discussed, for instance, in ferroelectric oxides.⁴⁴

We found S_2 , S'_3 , S_4 , S_6 , S_7 , S_{10} , S_{11} , S_{12} , and S_{13} states as in other surfaces. In particular, S_2 are Rashba split states whose dispersion has been fitted with parameters $\gamma_{SO} = (0.200 \pm 0.005) \times 10^{-9}$ eV cm and $m^*/m = (0.661 \pm 0.003)$. The S_8 Dirac-like states instead have not been found.

Along \bar{T} and \bar{T}' the spin polarization can rotate in a plane perpendicular to the high symmetry line: for the S'_3 , S_4 , and S_{10} states we followed this rotation as a function of k_{\parallel} . Some of them, as the S'_3 states, show a smooth behavior, while others (e.g. S_4 and S_{10}) have a more rapidly varying spin polarization, due to the anti-crossing and mixing of the states.

Compared to the recently studied Os(0001) surface, Re(0001) shows similar surface states and resonances, although they are higher in energy with respect to the Fermi level because of the lower number of electrons per atom. The main differences are found in the L states, which are more hybridized with the bulk, as shown by the planar average of the charge density. Minor differences can be observed in the spin textures of the S'_3 and S_4 states: in particular, the S_{4b} and S_{4c} states are ex-

changed with respect to those of Os(0001), as pointed out also by their symmetries.

Our work has been developed using the DFT-LDA scheme. The Kohn-Sham eigenvalues are different, in principle, from the quasi-particle energies, hence it might be necessary to compute many-body corrections for a more detailed comparison with experimental data. However, since these kinds of calculations are more computationally demanding, they are usually performed only when LDA is not enough to explain the experimental results. On the other surfaces, the main features of the bands, such as the presence or absence of L-gap states, are well predicted by DFT-LDA, while the exact energy positions of the surface states might have small shifts. To the best of our knowledge, there are no experimental data to compare with our results. We hope that our theoretical calculations could motivate ARPES measurements on this surface and, in case of discrepancies, other theoretical calculations.

ACKNOWLEDGMENTS

Computational facilities have been provided by SISSA through its Linux Cluster and ITCS and by CINECA through the SISSA-CINECA 2018 Agreement.

-
- ¹ A. Zangwill, *Physics at Surfaces*, Cambridge University Press, 1988.
 - ² G. Nicolay, F. Reinert, S. Hüfner, Spin-orbit splitting of the L-gap surface state on Au(111) and Ag(111), *Phys. Rev. B* 65 (2001) 033407.
 - ³ J. Henk, A. Ernst, P. Bruno, Spin polarization of the L-gap surface states on Au(111): a first-principles investigation, *Surf. Sci.* 566-568 (2004) 482.
 - ⁴ J. Henk, M. Hoesch, J. Osterwalder, A. Ernst, P. Bruno, Spin-orbit coupling in the L-gap surface states of Au(111): spin-resolved photoemission experiments and first-principles calculations, *J. Phys. Condens. Matter* 16 (2004) 7581-7597.
 - ⁵ R. Mazzarello, A. Dal Corso, E. Tosatti, Spin-orbit modifications and splittings of deep surface states on clean Au(111), *Surf. Sci.* 602, (2008) 893.
 - ⁶ S. Bornemann, O. Šipr, S. Mankovsky, S. Polesya, J. B. Staunton, W. Wurth, H. Ebert, J. Minár, Trends in the magnetic properties of Fe, Co, and Ni clusters and monolayers on Ir(111), Pt(111), and Au(111), *Phys. Rev. B* 86 (2012) 104436.
 - ⁷ R. Requist, Polina M. Sheverdyeva, Paolo Moras, Sanjoy K. Mahatha, Carlo Carbone, Erio Tosatti, Spin-orbit interaction and Dirac cones in d-orbital noble metal surface states, *Phys. Rev. B* 91 (2015) 045432.
 - ⁸ A. Dal Corso, Clean Ir(111) and Pt(111) electronic surface states: a first-principle fully relativistic investigation, *Surf. Sci.* 637-638 (2015) 106.
 - ⁹ A. Urru and A. Dal Corso, Clean Os(0001) electronic surface states: A first-principle fully relativistic investigation, *Surf. Sci.* 671 (2018) 17.
 - ¹⁰ S. Hüfner, *Photoelectron Spectroscopy*, third ed., Springer, Berlin, 2003.
 - ¹¹ S. LaShell, B. A. McDougall, E. Jensen, Spin Splitting of an Au(111) Surface State Band Observed with Angle Resolved Photoelectron Spectroscopy, *Phys. Rev. Lett.* 77 (1996) 3419.
 - ¹² F. Reinert, G. Nicolay, S. Schmidt, D. Ehm, S. Hüfner, Direct measurements of the L-gap surface states on the (111) face of noble metals by photoelectron spectroscopy, *Phys. Rev. B* 63 (2001) 115415.
 - ¹³ W. Di, K.E. Smith, S.D. Kevan, Angle-resolved photoemission study of the clean and hydrogen-covered Pt(111) surface, *Phys. Rev. B* 45 (1992) 3652.
 - ¹⁴ A. Ramstad, S. Raaen, N. Barrett, Electronic structure of the La-Pt(111) surface alloy, *Surf. Sci.* 448 (2000) 179.
 - ¹⁵ J. Wiebe, F. Meier, K. Hashimoto, G. Bihlmayer, S. Blügel, P. Ferriani, S. Heinze, R. Wiesendanger, Unoccupied surface state on Pt(111) revealed by scanning tunneling spectroscopy, *Phys. Rev. B* 72 (2005) 193406.
 - ¹⁶ E. Frantzeskakis, S. Pons, A. Crepaldi, H. Brune, K. Kern, M. Grioni, Ag-coverage-dependent symmetry of the electronic states of the Pt(111)-Ag-Bi interface: The ARPES view of a structural transition, *Phys. Rev. B* 84 (2011) 245443.
 - ¹⁷ I. Pletikosić, M. Kralj, D. Šokčević, R. Brako, P. Lazić, P. Pervan, Photoemission and density functional theory study of Ir(111); energy band gap mapping, *J. Phys. Condens. Matter* 22 (2010) 135006.
 - ¹⁸ A. Varykhalov, D. Marchenko, M.R. Scholz, E.D.L. Rienks, T.K. Kim, G. Bihlmayer, J. Sánchez-Barriga, O. Rader, Ir(111) Surface State with Giant Rashba Split-

- ting Persists under Graphene in Air, Phys. Rev. Lett. 108 (2012) 066804.
- ¹⁹ E. Starodub, A. Bostwick, L. Moreschini, S. Nie, F. El Gabaly, K.F. McCarty, E. Rotenberg, In-plane orientation effects on the electronic structure, stability, and Raman scattering of monolayer graphene on Ir(111), Phys. Rev. B 83 (2011) 125428.
 - ²⁰ Y.A. Bychkov, E.I. Rashba, Properties of a 2D electron gas with lifted spectral degeneracy, JETP Lett. 39 (1984) 78
 - ²¹ V. Pallassana, M. Neurock, L. B. Hansen, B. Hammer, J. K. Nørskov, Theoretical analysis of hydrogen chemisorption on Pd(111), Re(0001) and Pd_{ML}/Re(0001) Re_{ML}/Pd(111) pseudomorphic overlayers, Phys. Rev. B 60 (1999) 6146.
 - ²² E. Miniussi, E. R. Hernández, M. Pozzo, A. Baraldi, E. Vesselli, G. Comelli, S. Lizzit, D. Alfé, Non-local Effects on Oxygen-Induced Surface Core Level Shifts of Re(0001), J. Phys. Chem. C 116, 23297-23307.
 - ²³ J. Ontaneda, R. A. Bennett, R. Grau-Crespo, Electronic Structure of Pd Multilayers on Re(0001): The Role of Charge Transfer, J.Phys. Chem. C 119, 23436-23444.
 - ²⁴ H. Kim, A. Palacio-Morales, T. Posske, L. Rózsa, K. Palotás, L. Szunyogh, M. Thorwart, and R. Wiesendanger, Toward tailoring Majorana bound states in artificially constructed magnetic atom chains on elemental superconductors, Sci. Adv. 4, (2018) eaar5251.
 - ²⁵ P. Hohenberg, W. Kohn, Inhomogeneous Electron Gas, Phys. Rev. 136 (1964) B864.
 - ²⁶ W. Kohn, L. J. Sham, Self-Consistent Equations Including Exchange and Correlation Effects, Phys. Rev. 140 (1965) A1133.
 - ²⁷ P. Giannozzi, et al., QUANTUM ESPRESSO: a modular and open-source software project for quantum simulations of materials, J. Phys. Condens. Matter 21 (2009) 395502 (See <http://www.quantum-espresso.org>).
 - ²⁸ P. Giannozzi, et al., Advanced capabilities for materials modelling with Quantum ESPRESSO, J. Phys. Condens. Matter 29 (2017) 465901.
 - ²⁹ **thermo_pw** is an extension of the Quantum ESPRESSO (QE) package which provides an alternative organization of the QE work-flow for the most common tasks. For more information see https://dalcorsio.github.io/thermo_pw.
 - ³⁰ J. Perdew, A. Zunger, Self-interaction correction to density-functional approximations for many-electron systems, Phys. Rev. B 23 (1981) 5048.
 - ³¹ A. Dal Corso, Projector augmented-wave method: Application to relativistic spin-density functional theory, Phys. Rev. B 82 (2010) 075116.
 - ³² A. Dal Corso, Pseudopotentials periodic table: From H to Pu, Comp. Mat. Sci. 95 (2014) 337.
 - ³³ See <https://dalcorsio.github.io/pslibrary>.
 - ³⁴ R. W. G. Wyckoff, Crystal Structures 1 (1963) 7-83.
 - ³⁵ J. Monkhorst, J.D. Pack, Special points for Brillouin-zone integrations, Phys. Rev. B 13 (1976) 5188.
 - ³⁶ M. Methfessel, A.T. Paxton, High-precision sampling for Brillouin-zone integration in metals, Phys. Rev. B 40 (1989) 3616.
 - ³⁷ A band structure calculation of a 41-layers slab shows that the spin splittings decrease, but quite slowly: for instance, the splitting of the S'_3 states decreases of about 30 %.
 - ³⁸ H. Bentmann, T. Kuzumaki, G. Bihlmayer, S. Blügel, E. V. Chulkov, F. Reinert, and K. Sakamoto, Spin orientation and sign of the Rashba splitting in Bi/Cu(111), Phys. Rev. B 84 (2011) 115426.
 - ³⁹ L. Fu, Hexagonal Warping Effects in the Surface States of the Topological Insulator Bi₂Te₃, Phys. Rev. Lett. 103 (2009) 266801.
 - ⁴⁰ S. Basak, H. Lin, L. A. Wray, S.-Y. Xu, L. Fu, M. Z. Hasan, and A. Bansil, Spin texture on the warped Dirac-cone surface states in topological insulators, Phys. Rev. B 84 (2011) 121401.
 - ⁴¹ T. Oguchi, T. Shishidou, The surface Rashba effect: a $\mathbf{k} \cdot \mathbf{p}$ perturbation approach, J. Phys. Condens. Matter 21 (2009) 092001.
 - ⁴² I. Žutić, J. Fabian, and S. Das Sarma, Spintronics: Fundamentals and applications, Rev. Mod. Phys. 76 (2004) 323.
 - ⁴³ A. Manchon, H. C. Koo, J. Nitta, S. M. Frolov, and R. A. Duine, New perspectives for Rashba spin-orbit coupling, Nature Materials 14 (2015) 871.
 - ⁴⁴ H. Djani, A. C. Garcia-Castro, W. Tong, P. Barone, E. Bousquet, S. Picozzi, and P. Ghosez, Rashba spin-splitting in ferroelectric oxides: from rationalizing to engineering, arXiv:1903.0124v3.